Stabilization of Polynitrogen Anions in Tantalum-Nitrogen Compounds at High Pressure

Maxim Bykov, Elena Bykova, Alena V. Ponomareva, Igor Abrikosov, Stella Chariton, Vitali B. Prakapenka, Mohammad F. Mahmood, Leonid Dubrovinsky and Alexander F. Goncharov

Bykov, M., Bykova, E., Ponomareva, A. V., Abrikosov, I., Chariton, S., Prakapenka, V. B., Mahmood, M. F., Dubrovinsky, L., Goncharov, A. F., (2021), Stabilization of Polynitrogen Anions in Tantalum-Nitrogen Compounds at High Pressure, *Angewandte Chemie International Edition*.
https://doi.org/10.1002/anie.202100283

This article was published as:

M. Bykov *et al*. Agnewandte Chemie Int. Ed. 60(16), 9003-9008 (2021)

DOI: 10.1002/anie.202100283

Stabilization of polynitrogen anions in tantalum-nitrogen compounds at high pressure

Maxim Bykov,[a,b,*] Elena Bykova,[b] Alena V. Ponomareva,[c] Igor A. Abrikosov,[d] Stella Chariton,[e] Vitali B. Prakapenka,[e] Mohammad F. Mahmood,[a] Leonid Dubrovinsky,[f] Alexander F. Goncharov[b]

[a] Dr. Maxim Bykov, Prof. Dr. Mohammad Mahmood
Department of Mathematics, Howard University, Washington, DC 20059, USA
*E-mail: maks.byk@gmail.com

[b] Dr. Maxim Bykov, Dr. Elena Bykova, Dr. Alexander F. Goncharov
The Earth and Planets Laboratory, Carnegie Institution for Science, Washington, DC 20015, USA

[c] Dr. Alena V. Ponomareva
Materials Modeling and Development Laboratory, National University of Science and Technology 'MISIS', Moscow 119049, Russia

[d] Prof. Dr. Igor A. Abrikosov
Department of Physics, Chemistry and Biology (IFM), Linköping University, SE-58183 Linköping, Sweden

[e] Dr. Stella Chariton, Dr. Vitali B. Prakapenka
Center for Advanced Radiation Sources, University of Chicago, Lemont, IL 60437, USA

[f] Prof. Dr. Leonid Dubrovinsky
Bayerisches Geoinstitut, Bayreuth, 95447 Germany

Abstract: The synthesis of polynitrogen compounds is of great importance due to their potential as high energy density materials (HEDM), but because of the intrinsic instability of these compounds, their synthesis and stabilization is a fundamental challenge. Polymeric nitrogen units which may be stabilized in compounds with metals at high pressure are now restricted to non-branched chains with an average N-N bond order of 1.25, limiting their HEDM performances. Here we demonstrate the synthesis of a novel polynitrogen compound TaN_5 via a direct reaction between tantalum and nitrogen in a diamond anvil cell at ~100 GPa. TaN_5 is the first example of a material containing branched all-single-bonded nitrogen chains $[N_5^{5-}]_\infty$. Apart from that we discover two novel Ta-N compounds: TaN_4 with finite N_4^{4-} chains and incommensurately modulated compound TaN_{2-x}, which is recoverable at ambient conditions.

Introduction

Compounds containing polynitrogen species are considered ideal high energy density materials due to the significant energy release upon the transformation of single or double bonded nitrogen atoms to molecular nitrogen N_2. Consequently, such materials are very unstable and require specific synthesis techniques. Hitherto, only a few classes of compounds containing homonuclear polynitrogen species were stabilized at ambient conditions: azides (N_3^-)[1], diazenides and pernitrides (N_2^{x-})[2,3], pentazolates (N_5^-), [4,5], pentazenium (N^{5+}) salts[6], and most recently Mg_2N_4 containing *cis*-tetranitrogen (N_4^{4-})[7]. The application of pressure allows stabilizing polymeric nitrogen species either in nitrogen polymorphs like *cg*-N[8] and *bp*-N[9] or in compounds with metals (CsN_5[10], LiN_5[11], MgN_4[7], BeN_4[12], FeN_4[13,14], *etc*.). Recent experimental and theoretical studies suggest that the choice of metal significantly affects the resulting connectivity of polymeric or oligomeric nitrogen frameworks in high-pressure compounds and therefore it allows tuning the properties of the polynitrides [15–19]. For example, alkali metals form ionic pentazolate salts at high pressure[10,11], while some transition metals were shown to form metal-inorganic frameworks with predominantly polar-covalent bonding between metals and polymeric nitrogen linkers [20,21]. The diversity of polynitrogen species may be significantly increased in the compounds of early transition metals, which can combine both covalent and ionic components in the M-N bonds. Among binary transition metal nitrides, the highest thermodynamic stability is reached in groups 4 and 5 [22]. Particularly, tantalum has the largest number of different nitride compositions currently known. In this work we have studied the formation of polynitrides in the Ta-N system inspired by the richness of the Ta-N phase diagram at moderate pressures, which in turn may lead to diverse high-pressure polynitrides.

The binary Ta–N system displays a rich crystal chemistry, ranging from solid solutions of nitrogen in close-packed tantalum,[23] the subnitride β-Ta_2N,[24] several TaN polymorphs,[23,24] and nitrogen-rich phases Ta_5N_6[25], Ta_4N_5[25], Ta_2N_3[26,27], Ta_3N_5[28–30]. A number of theoretical and experimental works addressed the high-pressure phases in the Ta-N system. Zerr *et al*. synthesized recoverable η-Ta_2N_3 with U_2S_3-type structure (*Pbnm*) at 11 and 20 GPa by a decomposition of Ta_3N_5 in a large volume press. Friedrich *et al*. employed laser-heated diamond anvil cell to study direct chemical reactions between tantalum and nitrogen up to 27 GPa and identified β-Ta_2N and η-Ta_2N_3 in the reaction product.[31] Salamat *et al*. produced U_3Se_5 and U_3Te_5 polymorphs of Ta_3N_5 by a decomposition of the single-source amorphous precursor at 22 GPa in a laser-heated diamond anvil cell[29].

Theoretical studies show that N:Ta ratio of 5:3 as in Ta_3N_5 is not the limit for the Ta-N system[32]. Several TaN_2 polymorphs with $P4/mbm$[33], pyrite ($Pa\text{-}3$)[34], and $P6_3/mmc$[35] crystal

structures were considered in early theoretical calculations. Recently using particle swarm optimization methodology Xing *et al*. predicted that two thermodynamically stable TaN_2 polymorphs with *C*2/*m* and *Cmce* symmetries can be synthesized under pressures above 9 and 65 GPa, respectively. Alkhaldi and Kroll computed high-pressure phase diagram of the Ta-N system up to pressures of 140 GPa and temperatures up to 4000 K[36].

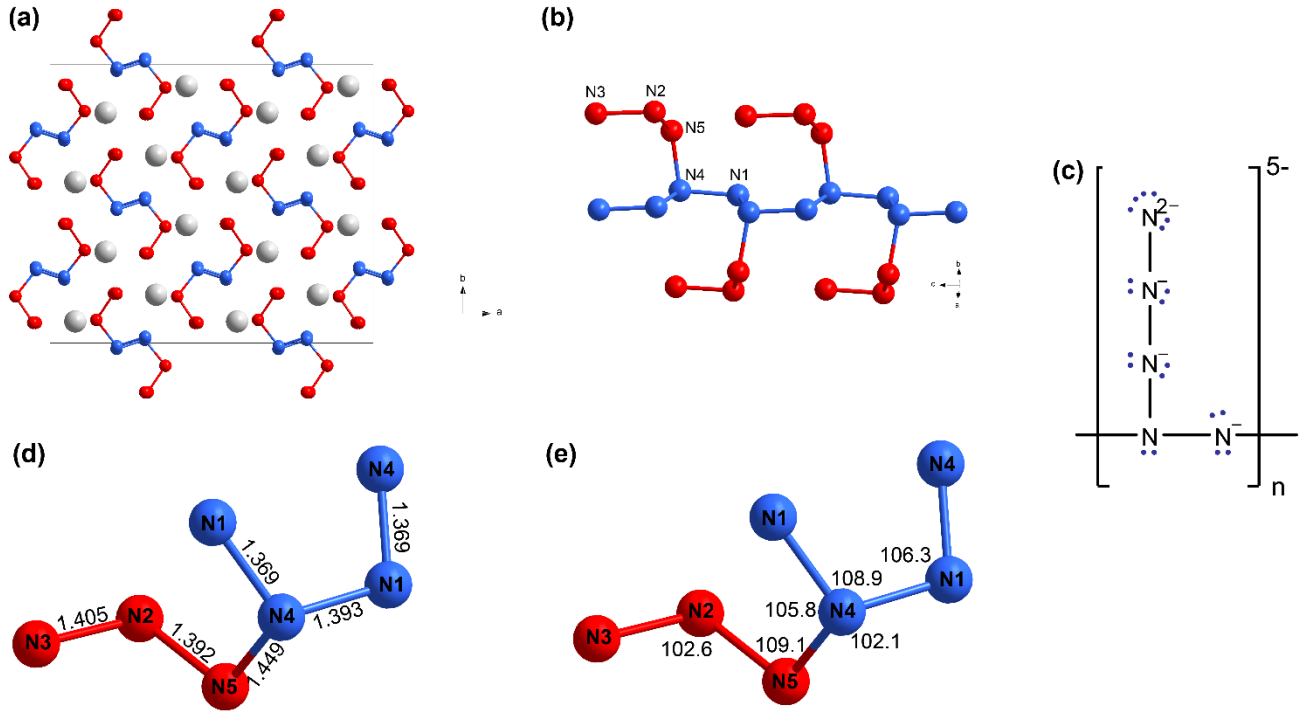

Figure 1. Crystal structure of TaN_5 at 102 GPa. Grey balls show the positions of Ta atoms, red and blue balls show the positions of nitrogen atoms of the branches and polymeric chains, respectively. (a) Projection along the c axis. (b) Polymeric nitrogen unit of TaN_5, (c) Lewis formula of the $[N_5^{5-}]_\infty$ anion. (d,e) N-N distances (Å) and N-N-N angles (º) within the polymeric unit of TaN_5.

As apparent from these calculations, more nitrogen rich tantalum nitrides may become stable at ultrahigh pressures, namely TaN_{10} (isostructural to other 5*d* metal polynitrides ReN_{10} and WN_{10} [20,21]), TaN_4 with finite-chain N_8^{10-} anions, and several TaN_2 polymorphs, which are mixed nitride-pernitride compounds like recently discovered rhenium nitride pernitride $Re_2(N_2)(N)_2$[37].

Here we have studied high-pressure reactions between Ta and N_2 in a laser-heated DAC at pressures well exceeding any previous experimental studies. We identify three novel compounds $TaN_{1.86}$ (at ~60 GPa), TaN_4 and TaN_5 (at ~100 GPa). $TaN_{1.86}$ possesses an incommensurately modulated structure, while TaN_4 and TaN_5 are polynitrides with N_4^{4-} finite and infinite branched

$[N_5]^{5-}_{\infty}$ chains, respectively. Due to the structural complexity, these compounds were never considered in prior theoretical calculations. Polynitrogen species in TaN_4 and TaN_5 are unprecedented in the series of transition metal polynitrides.

Results and Discussion

In all experiments described in this paper, a piece of Ta metal was placed inside a sample chamber of a diamond anvil cell, which was loaded with nitrogen, which served as a pressure-transmitting medium and as a reagent. Samples were compressed to target pressures and laser heated. The products of chemical reactions were studied by means of single-crystal and powder synchrotron X-ray diffraction. The summary of laser-heating experiments is given in the Table S1 and further details on the experimental methods and crystal structures are given in the Supporting Information and, Figs. S1-S3 and Table S2. The heating of Ta metal with nitrogen in a DAC at around 100 GPa and 2200(200) K resulted in the formation of two novel nitrogen-rich compounds TaN_4 and TaN_5 as determined from the single-crystal XRD analysis [38].

TaN_5 has an orthorhombic space group *Fdd*2 (No. 43) with 1 Ta and 5 N positions occupying Wyckoff sites 16*b*. Nitrogen atoms form unprecedented branched chain infinitely expanding along the **c**-axis (Fig. 1a,b). Each nitrogen atom possesses tetragonal coordination: N3 atoms are connected to 3Ta and 1N atoms, N1, N2, N5 have 2 Ta and 2N neighbors, while N4 atoms are connected to 1Ta and 3 N atoms. The bond angles ranging from 102.1 to 109.1º agree with the sp^3 hybridization and the N-N distances (1.369 – 1.449 Å) are in a good agreement with the single character of every N-N bond. In the ionic consideration, the polymeric $[N_5^{5-}]_{\infty}$ anion agrees with the common oxidation state of Ta(V) and should have the Lewis formula shown on the Fig. 1c.

The TaN_5 compound can be well rationalized within the extended 8-N Mooser Pearson rule. According to this rule, the average number of nitrogen-nitrogen bonds per nitrogen atom in a compound MNx is b(NN) = 8 – (e(M)+x·e(N))/x, where *e*(M) and *e*(N) are the numbers of valence electrons of metal and nitrogen, respectively. The calculation for TaN_5 gives *b*(NN) = 2, that agrees with the results of crystal-chemical analysis (1 N-N bond for N3, 3 for N4 and 2 for the rest of nitrogen atoms give 2 in average). Infinite nitrogen units were previously reported in FeN_4[13,14], BeN_4[12], $ReN_8{\cdot}N_2$[20], $Hf_4N_{20}{\cdot}N_2$, Hf_2N_{11}, $WN_8{\cdot}N_2$, $Os_5N_{28}{\cdot}N_2$[21] and MgN_4 compounds[7]. However, TaN_5 is a unique compound. First, the average N-N bond order is 1 (compared to 1.25 in other known polynitrides). Second, TaN_5 is the first example of the branched-chain structure unexpected for polynitrogen compounds.

To gain a deeper insight into the properties of the TaN_5, we performed theoretical calculations based on density functional theory (DFT). We carried out the full structure optimization from ambient to the synthesis pressure and found that optimized crystal structures are in a very good

agreement with the experimental ones. Calculated phonon dispersion relations show no imaginary frequencies demonstrating the dynamic stability of TaN_5 (Fig. 2a). The absence of high-frequency phonons (> 1250 cm^{-1}) agrees with the all-single-bonded nitrogen framework and with the experimental Raman spectrum (Fig. S4). According to theoretical calculations TaN_5 is a semiconductor, which is an expected behavior for a standard Zintl phase[39]. To determine the value of the band gap in TaN_5 calculations were performed using PBEsol and HSE06 methods. The estimated band gap E_g from the electronic density of state (DOS) (Fig. 2b) and band structure (Fig. S5) results obtained by the PBEsol method give E_g ~ 1.55 eV. The HSE06 DOS calculations (Fig. S6) give E_g = 3.00 eV. Both calculations give a low positive pressure band gap coefficient dE_g/dp < +2meV/GPa in the pressure range of 60-100 GPa. The calculation of the band structure by the PBEsol method showed that the band gap has an indirect character (Fig. S5).

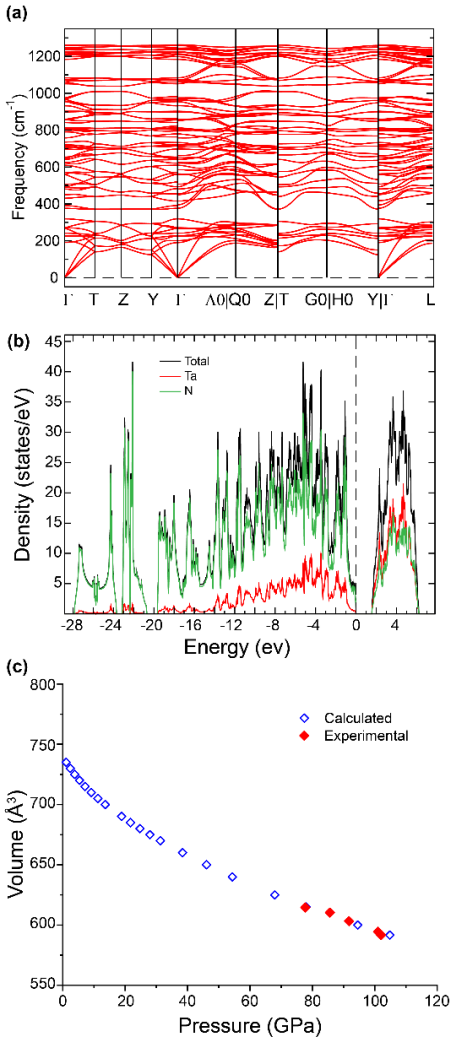

Figure 2. (a) Phonon spectra, (b) electronic densities of states of TaN_5 at ~102 GPa. (c) Calculated and experimental pressure-volume dependence of TaN_5 (can be described by the 4-th order Birch-Murnaghan equation of state with V_0 = 737.64 $Å^3$, K_0 = 205 GPa, K' = 11.22, K'' = -0.497 GPa^{-1}).

TaN_4 is found in a mixture with TaN_5 (Fig. S2), but forms separate well-crystallized grains suitable for the single-crystal XRD analysis. It crystallizes in the monoclinic space group $P2_1/n$ (No. 14) with 1 Ta and 4 N atoms at the general positions 4*e*. Nitrogen atoms form four-member chains (Fig. 3). The analysis of bond distances and angles suggests that N4 atoms have sp^2 hybridization with the N3-N4-N2 angle close to 120º. The N4-N2-N1 angle 109.1º is close to ideal tetrahedral angle, suggesting sp^3 hybridization of the N2 atom and single character of N4-N2 and N1-N2 bonds. The lengths of N4-N2 and N1-N2 bonds are very close to the nitrogen-nitrogen bond in *cg*-N at similar conditions[8]. The non-planar character of the N_4 unit excludes complete π-electron delocalization. Therefore, the N_4 anion can be viewed as a tetraz-1-enide anion $[N\text{-}N\text{-}N{=}N]^{4-}$ (Fig. 3c). Nevertheless, it should be pointed out that the N3-N4 bond length is only slightly shorter than the N1-N2 bond, while the former is supposed to be a double bond, and the latter is a single bond according to the Fig. 3c. Therefore, π-electron delocalization might occur in this polyanion to some extent, with the tetraz-1-enide anion $[N\text{-}N\text{-}N{=}N]^{4-}$ being the dominant resonance form. This bonding scheme is in a good agreement with the 8-N rule, with an average number of N-N bonds per nitrogen atoms equal to 2 and the oxidation state of Ta +IV. Calculated charge density maps (Fig. 3b) also show the increased charge density between N3 and N4 atoms compared to N2-N4 and N1-N2 pairs. Previously the N_4 units were observed in Mg_2N_4 compound, but unlike in TaN_4 those N_4 units are planar with a completely delocalized π-system[7].

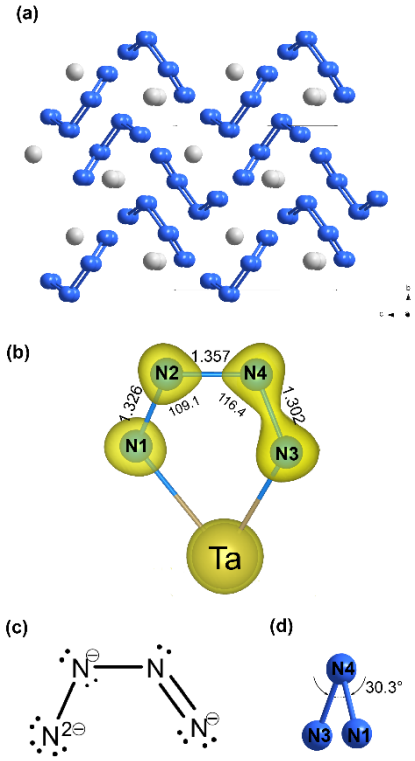

Figure 3. (a) Crystal structure of TaN_4 at 102 GPa. Blue and grey spheres show the positions of nitrogen and tantalum atoms respectively (b) Geometry of the N_4 structural unit with an overlay of calculated charge density distribution (c) Lewis structure of tetraz-1-enide anion (d) N_4 unit projected along N2-N4 direction.

The calculated phonon spectra of TaN_4 do not show any imaginary frequencies (Fig. S8a) and compared to TaN_5, a higher frequency phonon branch appears around 1400 cm^{-1} which agrees with the appearance of double or partially double nitrogen-nitrogen bonds in N_4^{4-} anions. According to our theoretical calculations TaN_4 exhibits metallic properties (Fig. S8b) with both Ta and N states contribution at the Fermi level, which is supported by the fact that TaN_4 is a d^1 system, *i.e.* some of the Ta levels might not be completely filled at the Fermi level and that the antibonding electronic levels of the N_4 anion are not saturated. From Fig. S5b we can see that the Fermi energy is located in a narrow DOS pseudogap that occurs due to the mixing of *d*-electrons Ta and mainly p_z-electrons N2, N3, N4 atoms and leads to the splitting of the band. The calculated band structure shows the pseudogap with points across the Fermi level along Γ-Z and C2-Y2 lines (Fig. S5b). Note, that the point along C2-Y2 line has a slightly gapped Dirac cone (~9 meV) character with a linear dispersion over a 0.8 eV energy.

As we briefly discussed above the sample containing a mixture of TaN_4 and TaN_5 produces a rich Raman spectrum (Fig. S4). As the TaN_4 compound is metallic it is not expected to possess strong Raman signal and according to the theoretical phonon dispersions, the highest frequency vibrations at Γ point should occur around 1400 cm^{-1}, which although overlap with the diamond Raman peak, would be, in principle, detectable if their intensity was comparable with other sample peaks at lower frequencies. Therefore, we assume that the major portion of Raman signal arises from TaN_5 with the highest frequencies around 1250 cm^{-1} in a good agreement with the calculated phonon dispersions (Fig. 2a and Fig. S4c). Due to the extreme complexity of the system with 96 atoms in the unit cell, the direct assignment of all Raman-active modes (69 modes: $17A_1 + 18A_2 + 17B_1 + 17B_2$) is a non-trivial task, however it is possible to qualitatively assign the regions of the Raman spectrum to certain types of vibrations. First, the spectrum has several high-frequency modes, which can be attributed to deformations and stretching of N-N modes and their combinations. Several broad bands at 400-600 cm^{-1} are the lattice modes of non-reacted molecular N_2, while the lattice modes at 200-400 cm^{-1} are likely the translations and rotations of big fragments of N-chains. The most valuable information from our Raman experiment is that the compound can be preserved in a DAC to pressures of at least 35 GPa (Fig. S4b,c). The possibility of quenching to ambient pressure is predicted by the calculated phonon dispersions at P = 0 GPa. As seen from Fig. S7 the phonon dispersion curves of TaN_5 and TaN_4 do not have imaginary modes at atmospheric pressure that suggests their dynamical stability at P = 0 GPa and T = 0 K.

Reheating of the partially decompressed TaN_4/TaN_5 sample at 61 GPa resulted in a drastic change of the diffraction pattern, which could be indexed with the tetragonal unit cell (a = b = 2.882(4), c = 5.728(6) Å) and two modulation vectors $\mathbf{q}_1$ = 0.305**a*** + 0.305**b*** + ½**c*** and $\mathbf{q}_2$ = -0.305**a*** + 0.305**b*** + ½**c***. Neither TaN_4 nor TaN_5 remained in the sample chamber after this heating. Structure solution of the incommensurate phase was successful in the superspace group $P4/nmm$(αα½)0000(-αα½)0000 (No. 129.2.69.14). The details of the structure refinement and final crystallographic model is given in the Supporting Information (Tables S5, S6, Fig. S9). The basic structure of the new compound TaN_{2-x} (x = 0.14) belongs to the Cu_2Sb structure type with Ta occupying the Wyckoff position 2c, while N1 atoms and N2 atoms occupy positions 2c and 2a, respectively. This structure does not contain covalent nitrogen-nitrogen bonds (Fig. 4). Formation of modulated structures due to non-stoichiometry is well documented for Cu_2Sb structure type, *e.g.* in $Cu_{3-x}Te_2$.[40] On decompression, $TaN_{1.86}$ remained in the sample chamber down to ambient pressure. It should be noted that the modulation **q**-vectors do not depend on pressure (Table S7), therefore the modulation is the intrinsic property of TaN_{2-x} related only to its non-stoichiometry, but not to any electronic or magnetic phenomena, which usually show pressure dependence [41–43].

The TaN_{2-x} compound was reproduced in a separate experiment where we consequently heated Ta in nitrogen atmosphere starting from 32 GPa. Below 60 GPa, we could not detect anything but η-Ta_2N_3 compound, previously known from the high-pressure experiments of Zerr *et al.*[26] and Friedrich *et al*. [31] Only after heating at ~62 GPa we could obtain $TaN_{1.86}$ in this experiment.

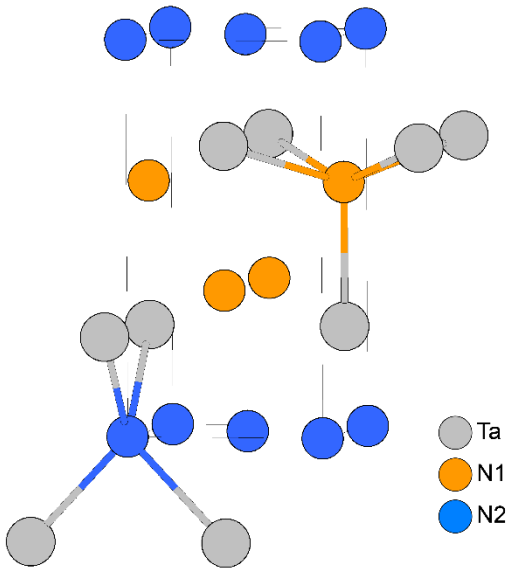

Figure 4. Average crystal structure of TaN_{2-x}

As the energy of the triple nitrogen-nitrogen bond is significantly larger than that of double and single bonds, the decomposition of polynitrides to metal-rich nitrides and nitrogen is a very exothermic process. Therefore, polynitrides are often considered as high-energy density materials. In order to get the lower estimate of the volumetric and gravimetric energy densities (VED and GED) of TaN_4 and TaN_5, we have calculated the enthalpy of the decomposition of both compounds to the next most nitrogen-rich tantalum nitride Ta_3N_5 and nitrogen:

$$6TaN_4 \rightarrow 2Ta_3N_5 + 7N_2\uparrow$$

$$3TaN_5 \rightarrow Ta_3N_5 + 5N_2\uparrow$$

The temperature contribution at T=298 K to the Gibbs energy of TaN_4, TaN_5 and Ta_3N_5 was obtained through the phonon entropy considered in the framework of the Debye–Gruneisen model[44] combined with *ab initio* calculations. The enthalpy and entropy of N_2 at T=298 K were obtained from thermochemical tables[45]. With GED (TaN_4) = 1.31 kJ/g, VED(TaN_4) = 12.3 kJ/cm^3, GED (TaN_5) = 2.02 kJ/g, VED (TaN_5) = 18.0 kJ/cm^3. Due to the high density of both TaN_4 and

TaN_5, they possess extremely high volumetric energy density that is higher than the typical energy density of TNT, PETN (7.2 and 10.6 kJ/cm^3) [46]. The decomposition to more tantalum-rich nitrides like TaN would result in even higher energy release. Since Ta is a heavy metal, TaN_4 and TaN_5 possess low GED, but very high VED. The energetics of the polynitride is primarily defined by the nitrogen contents, *i.e.*, the recalculation of the energy density into the kJ/mol would be close for many compounds even containing different metals. Therefore, the variation of the metal can allow achieving the desired balance between GED and VED for practical applications.

Conclusion

To conclude, in this study we have synthesized and characterized three novel compounds in the Ta-N system (Fig. 5). TaN_4 and TaN_5 possess unprecedented nitrogen units which were never observed before. TaN_5 contains branched polymeric nitrogen chains and it is the first polynitride, with all single-bonded nitrogen atoms. The complex non-stoichiometric $TaN_{1.86}$ could be quenched at ambient conditions, while the lowest pressure reached for TaN_4 and TaN_5 was around 35 GPa in this study. The formation of branched [N_5^{5-}] chains in TaN_5 demonstrates the potential of electropositive transition metals to stabilize complex single-bonded homopolyatomic anions. This is made possible due to several specific properties of Ta. First, as a group 5 metal, Ta has access to a variety of oxidation states up to +5 and due to relatively low electronegativity, even the highest oxidation states may be reached in compounds with nitrogen. The latter effect is well demonstrated by a comparison of Ta with other 5*d* metals (W, Re, Os), which form compounds with nitrogen at ~100 GPa, where metals achieve only the oxidation state of +4 (WN_{10}, ReN_{10}, Os_5N_{34}) despite the wider range of possible oxidation states of W, Re and Os compared to Ta[20,21]. Secondly, the stabilization of complex polyanions requires a metal to have large coordination numbers: Ta is 10-fold coordinated in TaN_5 and 9-coordinated in TaN_4, which would not be possible for the 3*d* metals. Lastly, the Ta-N compounds should occupy intermediate position between ionic alkali or alkaline-earth metal polynitrides (anions are stabilized by resonance, M-N bonds are ionic) and polar covalent transition metal polynitrides (anions destabilized by the distortion imposed by polar covalent M-N bonds like in FeN_4), which leads to novel structure types. Interestingly, we could not find any compounds that naturally link nitrides and polynitrides, namely the compounds containing dinitrogen anions [N_2]$^{x-}$. Such species are common among transition metal (OsN_2,[47] PtN_2,[3] RhN_2,[48] etc.), main-group element (SiN_2, GeN_2, SnN_2[49]), alkali and alkaline-earth (BaN_2,[50] SrN_2,[2] NaN_2[51]) dinitrides. Therefore, these phases can still be hidden between 62 and 100 GPa. Non-stoichiometric $TaN_{1.86}$ is the new most nitrogen-rich tantalum nitride, which is available at ambient conditions.

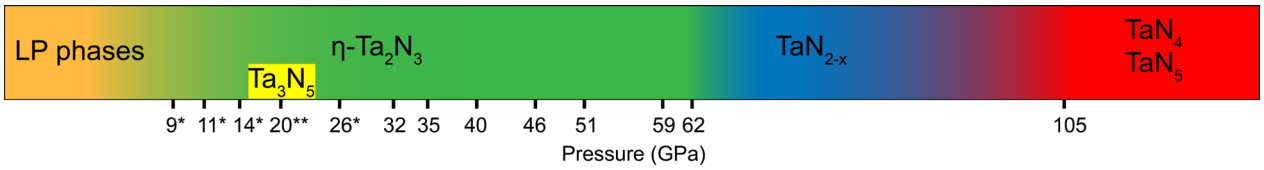

Figure 5. Summary of high-pressure experiments in the Ta-N system. Pressures at which laser-heating was performed are marked on the horizontal axis. Asterisks * indicate the experiments reported by Friedrich *et al*.[31], ** indicate the experiments of Salamat *et al*.[29] on the synthesis of Ta_3N_5 from single-source precursor. Pressures of the experiments of Zerr *et al*. in a multianvil apparatus[26] coincide with those from Friedrich *et al*. All experiments above 30 GPa are from this study.

Acknowledgements

Research was sponsored by the US Army Research Office and was accomplished under the Cooperative Agreement Number W911NF-19-2-0172. L.D. thank the Deutsche Forschungsgemeinschaft (DFG projects DU 954-11/1 and, DU 393-9/2, and DU 393-13/1) and the Federal Ministry of Education and Research, Germany (BMBF, grant no. No. 05K19WC1) for financial support. Theoretical analysis of chemical bonding was supported by the Ministry of Science and Higher Education of the Russian Federation in the framework of Increase Competitiveness Program of NUST MISIS (No. K2-2020-026) implemented by a governmental decree dated 16 March 2013, No. 211. Support from the Swedish Government Strategic Research Area in Materials Science on Functional Materials at Linköping University (Faculty Grant SFO-Mat-LiU No. 2009 00971), Knut and Alice Wallenberg Foundation (Wallenberg Scholar Grant No. KAW-2018.0194) and the Swedish Research Council (VR) grant No. 2019-05600 is gratefully acknowledged. This research used resources of the Advanced Photon Source, a U.S. Department of Energy (DOE) Office of Science User Facility operated for the DOE Office of Science by Argonne National Laboratory under Contract No. DE-AC02-06CH11357

Keywords: nitrides • polynitrides • tantalum nitride • high energy density materials • high pressure

[1] T. Curtius, *Berichte der Dtsch. Chem. Gesellschaft* **1890**, *23*, 3023–3033.

[2] G. Auffermann, Y. Prots, R. Kniep, *Angew. Chem. Int. Ed.* **2001**, *40*, 547–549; *Angew. Chem*. **2001**, 113, 565-567

[3] J. C. Crowhurst, A. F. Goncharov, B. Sadigh, J. M. Zaug, D. Aberg, Y. Meng, V. B. Prakapenka, *J. Mater. Res.* **2008**, *23*, 1–5.

[4] C. Zhang, C. Yang, B. Hu, C. Yu, Z. Zheng, C. Sun, *Angew. Chem. Int. Ed.* **2017**, *56*, 4512–4514; *Angew. Chem*. **2017**, 129, 4583-4585

[5] Y. Xu, Q. Wang, C. Shen, Q. Lin, P. Wang, M. Lu, *Nature* **2017**, *549*, 78–81.

[6] K. O. Christe, W. W. Wilson, J. A. Sheehy, J. A. Boatz, *Angew. Chem. Int. Ed.* **1999**, *38*, 2004–2009; *Angew. Chem*. **1999**, 111, 2112-2118

[7] D. Laniel, B. Winkler, E. Koemets, T. Fedotenko, M. Bykov, E. Bykova, L. Dubrovinsky, N. Dubrovinskaia, *Nat. Commun.* **2019**, *10*, 4515.

[8] M. I. Eremets, A. G. Gavriliuk, I. A. Trojan, D. A. Dzivenko, R. Boehler, *Nat. Mater.* **2004**, *3*, 558–63.

[9] D. Laniel, B. Winkler, T. Fedotenko, A. Pakhomova, S. Chariton, V. Milman, V. Prakapenka, L. Dubrovinsky, N. Dubrovinskaia, *Phys. Rev. Lett.* **2020**, *124*, 216001.

[10] B. A. Steele, E. Stavrou, J. C. Crowhurst, J. M. Zaug, V. B. Prakapenka, I. I. Oleynik, *Chem. Mater.* **2017**, *29*, 735–741.

[11] D. Laniel, G. Weck, G. Gaiffe, G. Garbarino, P. Loubeyre, *J. Phys. Chem. Lett.* **2018**, *9*, 1600–1604.

[12] M. Bykov, T. Fedotenko, S. Chariton, D. Laniel, K. Glazyrin, M. Hanfland, J. S. Smith, V. B. Prakapenka, M. F. Mahmood, A. F. Goncharov, et al., arXiv:2010.15774.

[13] M. Bykov, E. Bykova, G. Aprilis, K. Glazyrin, E. Koemets, I. Chuvashova, I. Kupenko, C. McCammon, M. Mezouar, V. Prakapenka, et al., *Nat. Commun.* **2018**, *9*, 2756.

[14] M. Bykov, S. Khandarkhaeva, T. Fedotenko, P. Sedmak, N. Dubrovinskaia, L. Dubrovinsky, *Acta Crystallogr. Sect. E Crystallogr. Commun.* **2018**, *74*, 1392–1395.

[15] J. Zhang, A. R. Oganov, X. Li, H. Niu, *Phys. Rev. B* **2017**, *95*, 020103.

[16] A. G. Kvashnin, A. R. Oganov, A. I. Samtsevich, Z. Allahyari, *J. Phys. Chem. Lett.* **2017**, *8*, 755–764.

[17] B. A. Steele, I. I. Oleynik, *Chem. Phys. Lett.* **2016**, *643*, 21–26.

[18] S. Wei, D. Li, Z. Liu, X. Li, F. Tian, D. Duan, B. Liu, T. Cui, *Phys. Chem. Chem. Phys.* **2017**, *19*, 9246–9252.

[19] Z. Zhao, K. Bao, D. Li, D. Duan, F. Tian, X. Jin, C. Chen, X. Huang, B. Liu, T. Cui, *Sci. Rep.* **2014**, *4*, 4797.

[20] M. Bykov, E. Bykova, E. Koemets, T. Fedotenko, G. Aprilis, K. Glazyrin, H.-P. P. Liermann, A. V. Ponomareva, J. Tidholm, F. Tasnádi, et al., *Angew. Chem. Int. Ed.* **2018**, *57*, 9048–9053; *Angew. Chem*. **2018**, 130, 9186-9191.

[21] M. Bykov, S. Chariton, E. Bykova, S. Khandarkhaeva, T. Fedotenko, A. V. Ponomareva, J. Tidholm, F. Tasnádi, I. A. Abrikosov, P. Sedmak, et al., *Angew. Chem. Int. Ed.* **2020**, *59*, 10321–10326; *Angew. Chem*. **2020**, 132, 10407-10412.

[22] P. Höhn, R. Niewa, in *Handb. Solid State Chem.*, Wiley-VCH Verlag GmbH & Co. KGaA, Weinheim, Germany, **2017**, pp. 251–359.

[23] N. Schönberg, W. G. Overend, A. Munthe-Kaas, N. A. Sörensen, *Acta Chem. Scand.* **1954**, *8*, 199–203.

[24] L. E. Conroy, A. N. Christensen, *J. Solid State Chem.* **1977**, *20*, 205–207.

[25] A. Fontbonne, J.-C. Gilles, *Rev. Int. des Hautes Temp. des Refract.* **1969**, *6*, 181–191.

[26] A. Zerr, G. Miehe, J. Li, D. A. Dzivenko, V. K. Bulatov, H. Höfer, N. Boifan-Casanova, M. Fialin, G. Brey, T. Watanabe, et al., *Adv. Funct. Mater.* **2009**, *19*, 2282–2288.

[27] A. Y. Ganin, L. Kienle, G. V. Vajenine, *Eur. J. Inorg. Chem.* **2004**, *2004*, 3233–3239.

[28] J. Strahle, *Z. Anorg. Allg. Chem.* **1973**, *402*, 47–57.

[29] A. Salamat, K. Woodhead, S. I. U. Shah, A. L. Hector, P. F. McMillan, *Chem. Commun.* **2014**, *50*, 10041–10044.

[30] P. Kroll, T. Schröter, M. Peters, *Angew. Chem. Int. Ed.* **2005**, *44*, 4249–4254; *Angew. Chem*. **2005**, 117, 4321-4326.

[31] A. Friedrich, B. Winkler, L. Bayarjargal, E. A. Juarez Arellano, W. Morgenroth, J. Biehler, F. Schröder, J. Yan, S. M. Clark, *J. Alloys Compd.* **2010**, *502*, 5–12.

[32] D. Li, F. Tian, D. Duan, K. Bao, B. Chu, X. Sha, B. Liu, T. Cui, *RSC Adv.* **2014**, *4*, 10133–10139.

[33] H. Yan, M. Zhang, Q. Wei, P. Guo, *J. Alloys Compd.* **2013**, *581*, 508–514.

[34] S. K. R. Patil, N. S. Mangale, S. V. Khare, S. Marsillac, *Thin Solid Films* **2008**, *517*, 824–827.

[35] G. Soto, *Comput. Mater. Sci.* **2012**, *61*, 1–5.

[36] H. Alkhaldi, P. Kroll, *J. Phys. Chem. C* **2020**, *124*, 22221–22227.

[37] M. Bykov, S. Chariton, H. Fei, T. Fedotenko, G. Aprilis, A. V. Ponomareva, F. Tasnádi, I. A. Abrikosov, B. Merle, P. Feldner, et al., *Nat. Commun.* **2019**, *10*, 2994.

[38] CSD 2038294-2038296 contain supplementary crystallographic data for this paper. These data can be obtained free of charge from the joint CCDC's and FIZ Karlsruhe's service to view and retrieve structures via https://www.ccdc.cam.ac.uk/structures/

[39] R. Nesper, *Zeitschrift für Anorg. und Allg. Chemie* **2014**, *640*, 2639–2648.

[40] W. J. Schutte, J. L. de Boer, *Acta Crystallogr. Sect. B Struct. Sci.* **1993**, *49*, 398–403.

[41] M. Bykov, E. Bykova, L. Dubrovinsky, M. Hanfland, H.-P. Liermann, S. van Smaalen, *Sci. Rep.* **2015**, *5*, 9647.

[42] M. Bykov, J. Zhang, A. Schönleber, A. Wölfel, *Phys. Rev. B* **2013**, *88, 184420*.

[43] M. Bykov, E. Bykova, M. Hanfland, H.-P. Liermann, R. K. Kremer, R. Glaum, L. Dubrovinsky, S. van Smaalen, *Angew. Chem. Int. Ed.* **2016**, *55*, 15053–15057; *Angew. Chem*. **2016**, 128, 15277-15281.

[44] V. L. Moruzzi, J. F. Janak, K. Schwarz, *Phys. Rev. B* **1988**, *37*, 790–799.

[45] D. R. Stull, H. Prophet, Eds. , *JANAF Thermo- Chemical Tables*, National Bureau Of Standards, **1971**.

[46] B. M. Dobratz, *LLNL Explosives Handbook: Properties of Chemical Explosives and Explosives and Explosive Simulants*, **1981**.

[47] A. F. Young, C. Sanloup, E. Gregoryanz, S. Scandolo, R. J. Hemley, H. Mao, *Phys. Rev. Lett.* **2006**, *96*, 155501.

[48] M. Bykov, K. V. Yusenko, E. Bykova, A. Pakhomova, W. Kraus, N. Dubrovinskaia, L. Dubrovinsky, *Eur. J. Inorg. Chem.* **2019**, *2019*, 3667–3671.

[49] K. Niwa, H. Ogasawara, M. Hasegawa, *Dalt. Trans.* **2017**, *46*, 9750–9754.

[50] G. V. Vajenine, G. Auffermann, Y. Prots, W. Schnelle, R. K. Kremer, A. Simon, R. Kniep, *Inorg. Chem.* **2001**, *40*, 4866–4870.

[51] M. Bykov, K. R. Tasca, I. G. Batyrev, D. Smith, K. Glazyrin, S. Chariton, M. Mahmood, A. F. Goncharov, *Inorg. Chem.* **2020**, *59*, 14819–14826.

Experiment

In all experiments discussed in this paper a piece of Ta metal (Alfa Aesar, purity 99.95%) was placed inside a sample chamber of a BX90 diamond anvil cell and loaded with nitrogen that served as a reagent and as a pressure-transmitting medium. The samples were compressed to target pressures and laser-heated using double-sided laser-heating systems of the beamline GSECARS (APS, Argonne, USA) and Bayerisches Geoinsitute (BGI, Bayreuth, Germany). The summary of samples and laser-heating conditions are summarized in the Table S1. In X-ray diffraction (XRD) experiments, pressure was determined using the equation of state of Ta (Vinet EoS, V_0 = 18.035 Å^3, K_0 = 194 GPa, K_0' = 3.52 according to the ref. [1]). For Raman experiments we used the shift of the diamond Raman peak to determine pressure[2].

The reaction products contained multiple good-quality single-crystalline domains of novel phases and they were studied by synchrotron single-crystal X-ray diffraction at the beamline GSECARS 13IDD (APS, Argonne, USA). The following beamline setup was used: λ = 0.2952 Å, beam size ~3×3 μm^2, Pilatus CdTe 1M detector. For the single-crystal XRD measurements samples were rotated around a vertical ω-axis in a range ±36°. The diffraction images were collected with an angular step Δω = 0.5° and an exposure time of 1-2s/frame. For analysis of the single-crystal diffraction data (indexing, data integration, frame scaling and absorption correction) we used the *CrysAlis^{Pro}* software package. To calibrate an instrumental model in the *CrysAlis^{Pro}* software, *i.e.*, the sample-to-detector distance, detector's origin, offsets of goniometer angles, and rotation of both X-ray beam and the detector around the instrument axis, we used a single crystal of orthoenstatite ($(Mg_{1.93}Fe_{0.06})(Si_{1.93}, Al_{0.06})O_6$, *Pbca* space group, a = 8.8117(2), b = 5.18320(10), and c = 18.2391(3) Å). The same calibration crystal was used at both beamlines. Powder diffraction measurements were performed either without sample rotation (still images) or upon continuous rotation in the range ±20°ω. The images were integrated to powder patterns with DIOPTAS software[3]. Le-Bail fits of the diffraction patterns were performed with the Jana2006 software. The structure was solved with the ShelXT structure solution program[4] using intrinsic phasing and refined with the Jana2006 and Olex2 programs[5,6]. CSD 2038294-2038296 contain the supplementary crystallographic data for this paper. These data can be obtained free of charge from FIZ Karlsruhe *via* www.ccdc.cam.ac.uk/structures. Some experimental details, crystal structures, raw data are also summarized in the Figures S1-S3 and Tables S1-S6.

Details of the structure refinement of TaN_{2-x}

For the structure refinement of TaN_{2-x}, the modulation functions u_i^{μ} were described as harmonic waves of first order according to van Smaalen *et al.* [7] in the following form:

$$u_i^{\mu}(\bar{x}_4, \bar{x}_5) = A_i^{10}(\mu)\sin[2\pi\bar{x}_4] + B_i^{10}(\mu)\cos[2\pi\bar{x}_4] + \\ + A_i^{01}(\mu)\sin[2\pi\bar{x}_5] + + B_i^{01}(\mu)\cos[2\pi\bar{x}_5] \quad (1),$$

where $A^{10}(\mu), A^{01}(\mu), B^{10}(\mu), B^{01}(\mu)$ are the modulation amplitudes of the atom μ, $\bar{x}_4 = t + \boldsymbol{q_1} \cdot \bar{\boldsymbol{x}}, \bar{x}_5 = u + \boldsymbol{q_2} \cdot \bar{\boldsymbol{x}}, i = x, y, z$. The occupation modulation for the atom N1 was described by a harmonic function of the first order:

$$p_{N1}(\bar{x}_4, \bar{x}_5) = P^0(1 + P_s^{10} \sin[2\pi\bar{x}_4] + P_c^{10} \cos[2\pi\bar{x}_4] + P_s^{01} \sin[2\pi\bar{x}_5] + P_c^{01} \cos[2\pi\bar{x}_5]) \quad (2),$$

where $P_s^{10}, P_c^{10}, P_s^{01}, P_c^{01}$ are the modulation amplitudes, and P^0 is the average occupation of the N1 atom. Structure refinement with varied occupancies for all atoms did not show the significant deviations of Ta and N2 atom occupancies from 1.

Calculations details

The *ab initio* calculations of TaN_4 and TaN_5 were performed using the all electron projector-augmented-wave (PAW) method as implemented in the VASP code [8–10]. To obtain structural and electronic properties under hydrostatic pressure have we used the generalized gradient approximation with the Perdew-Burke-Ernzerhof for solids (PBEsol) exchange-correlation functional [11]. We also used the nonlocal screened Coulomb potential hybrid density Heyd-Scuseria-Ernzerhof (HSE06) functional to estimate the band gap for TaN_5 [12,13]. The HSE06 functionality is used by mixing 75% PBE exchange with 25% Hartree-Fock exchange and 100% PBE correlation.

The sampling for Brillouin zone integrations is performed using the Gamma scheme with 18x14x14 (TaN_4) and 15x6x6 (TaN_5) k-point grids for PBEsol and 5×5×5 k-point grids for HSE06 (TaN_5, primitive cell). The energy cutoff for the plane waves included in the expansion of wave functions was set to 700 eV. The convergence criterion for the electronic subsystem has been chosen to be equal to 10^{-5} eV for two subsequent iterations, and the ionic relaxation loop within the conjugated gradient method was stopped when forces became of the order of 10^{-4} eV/Å.

The phonon calculations have been performed within quasiharmonic approximation at temperature T=0 K using the finite displacement approach implemented into PHONOPY software [14]. A (2x2x2) sized supercell had to be applied with 9x9x7 (TaN_4) and 7x7x7 (TaN_5) k-point grids. For TaN5 the long-range interaction of the macroscopic electric field induced by polarization of collective ionic motions near the point Γ was obtained by adding a nonanalytical term to the dynamical matrix by determining the Born effective charges and dielectric tensors [15–17].

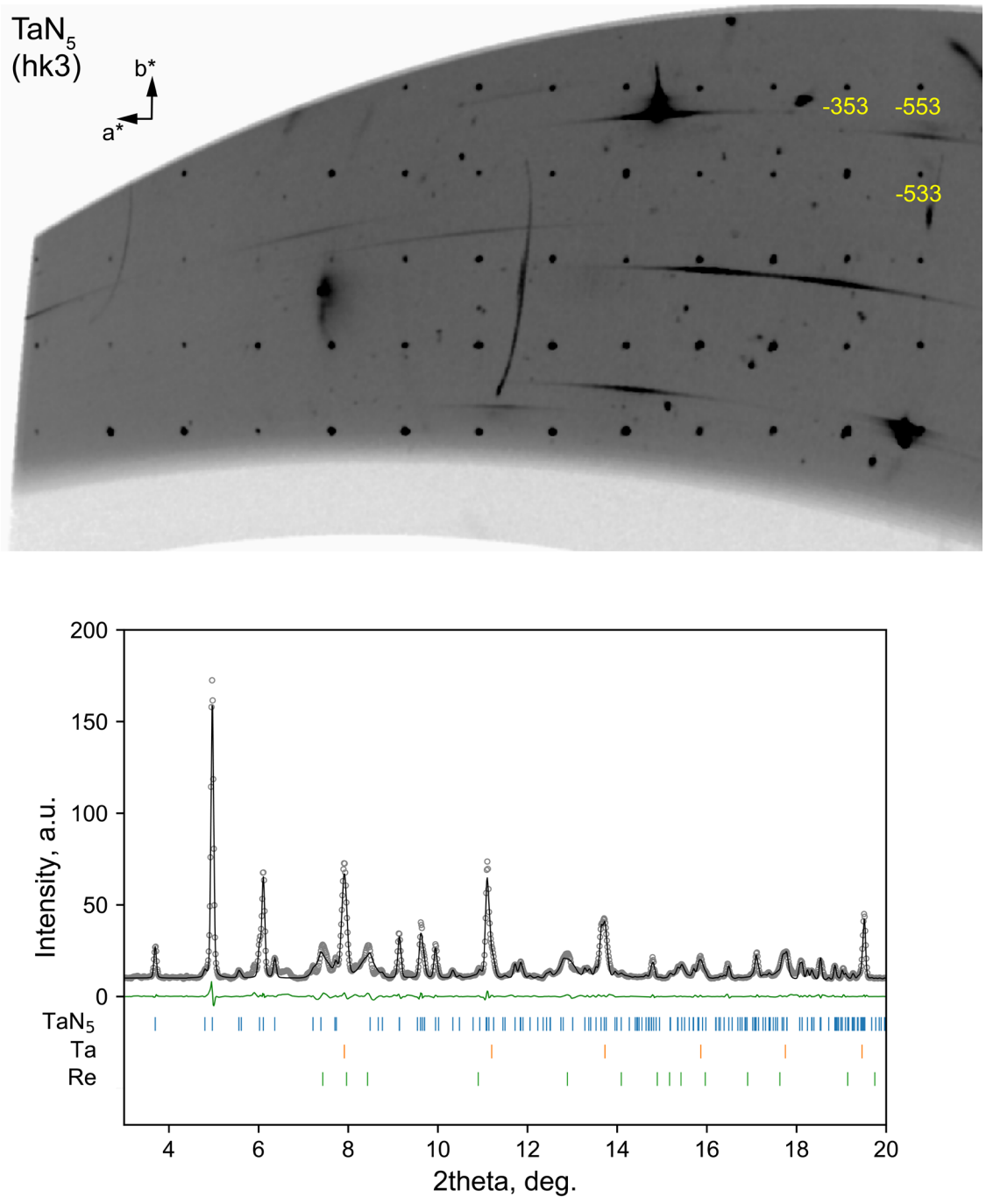

Figure S1. Reconstructed (*hk*3) reciprocal lattice plane of TaN_5 at ~102 GPa and corresponding powder diffraction pattern with a Le-Bail fit.

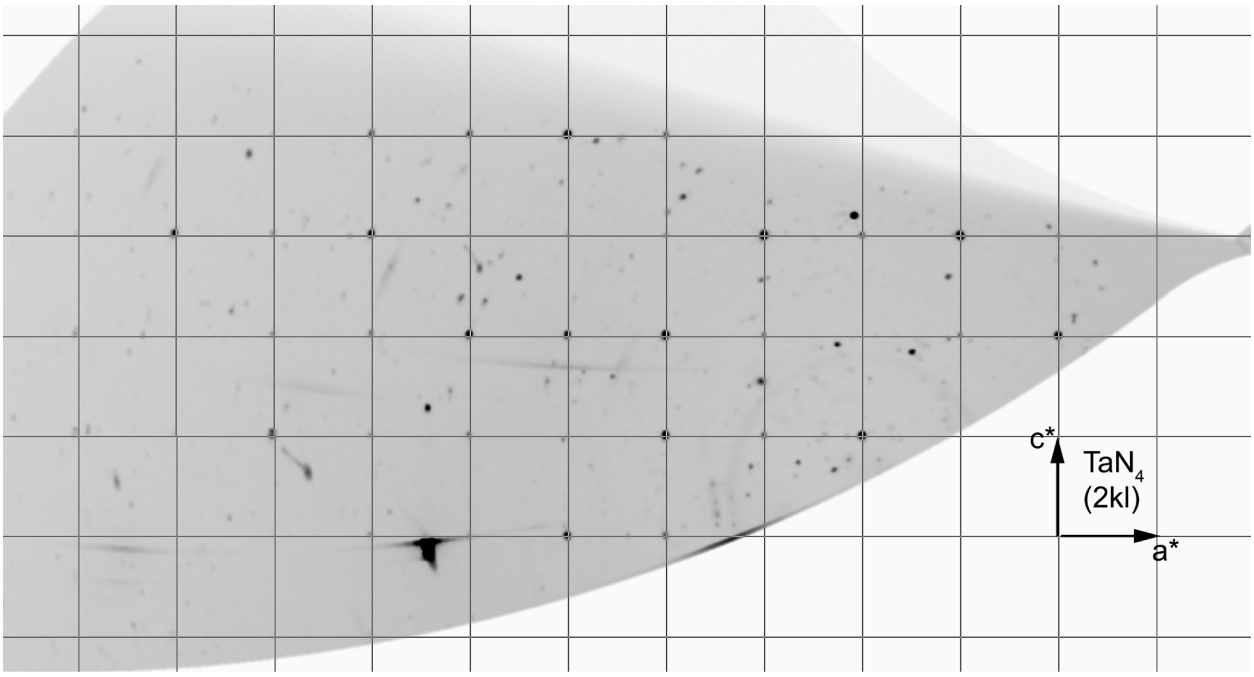

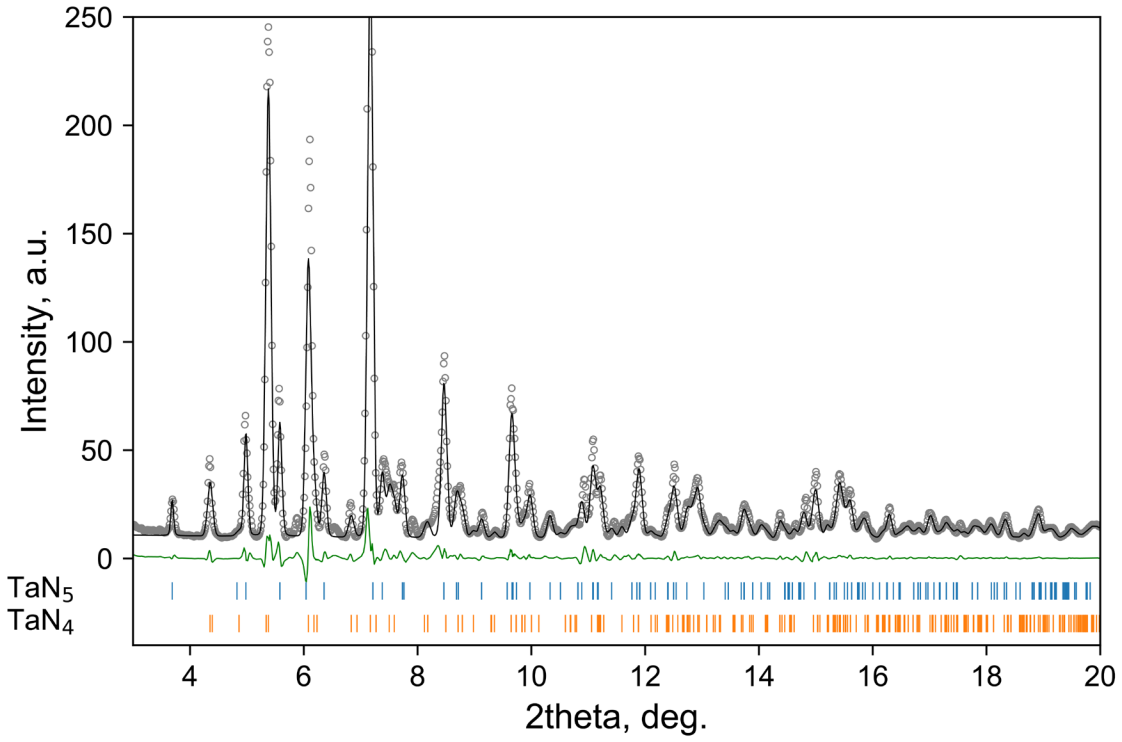

Figure S2. Reconstructed (*2kl*) reciprocal lattice plane of TaN_4 at ~102 GPa and corresponding powder diffraction pattern with a Le-Bail fit.

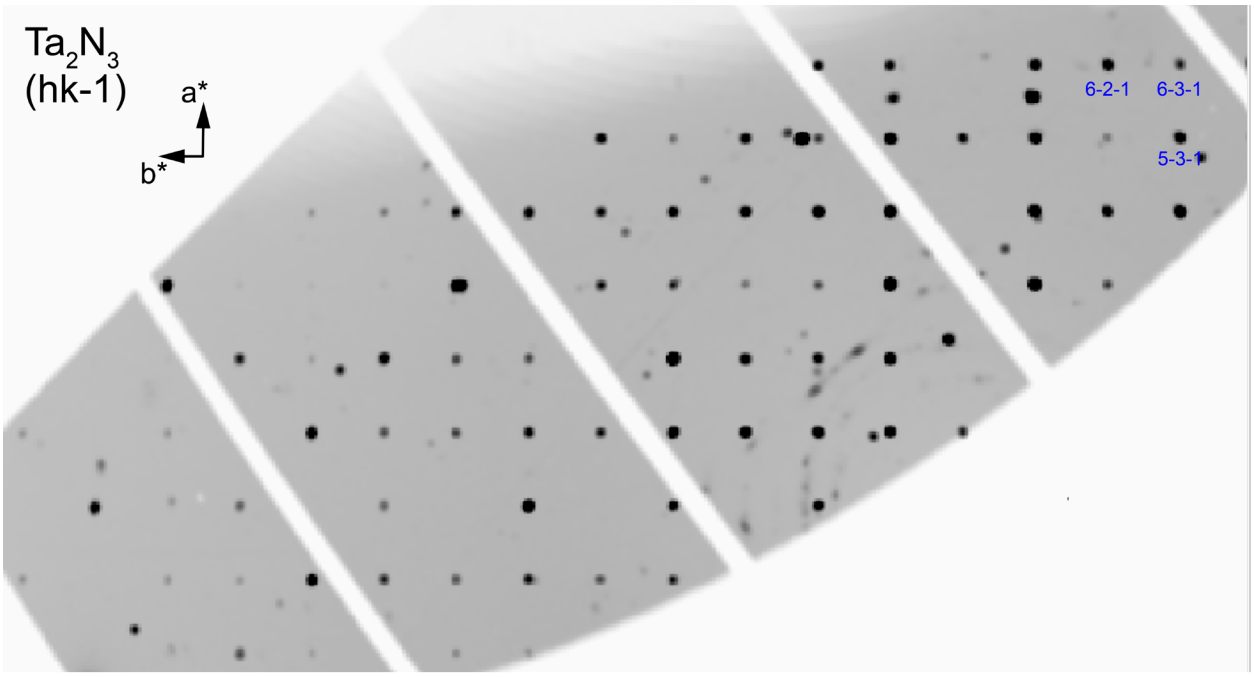

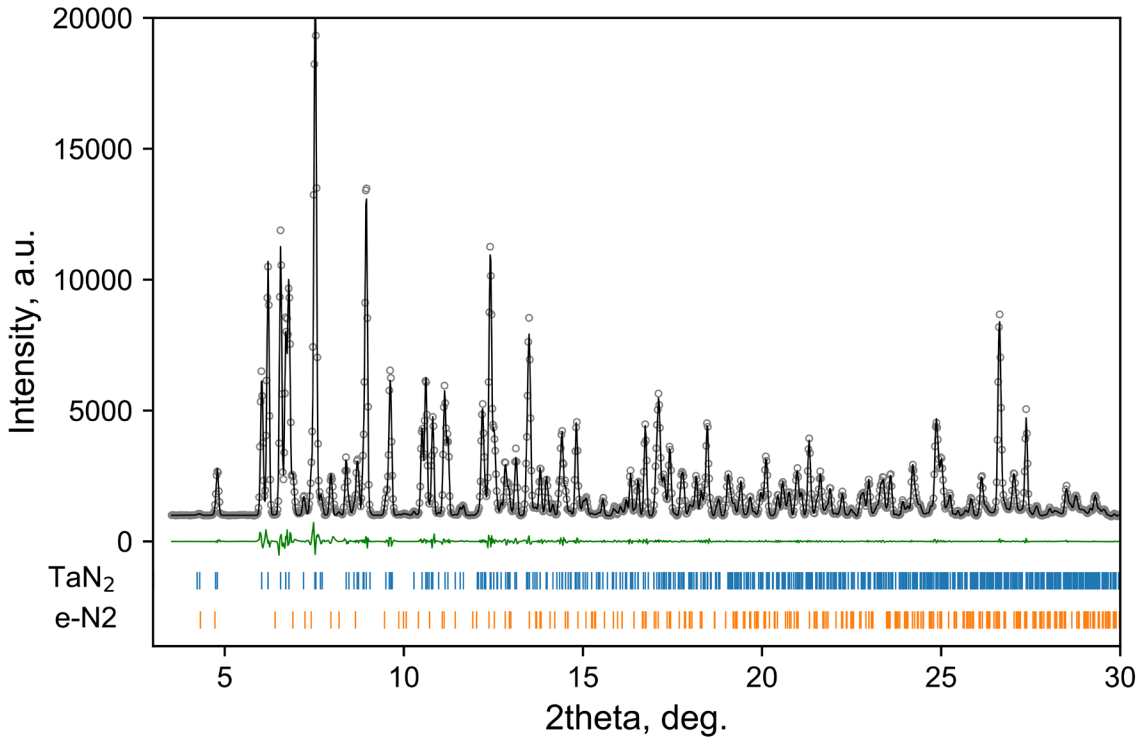

Figure S3. Reconstructed (*hk*-1) reciprocal lattice plane of Ta_2N_3 at ~32 GPa and corresponding powder diffraction pattern with a Le-Bail fit.

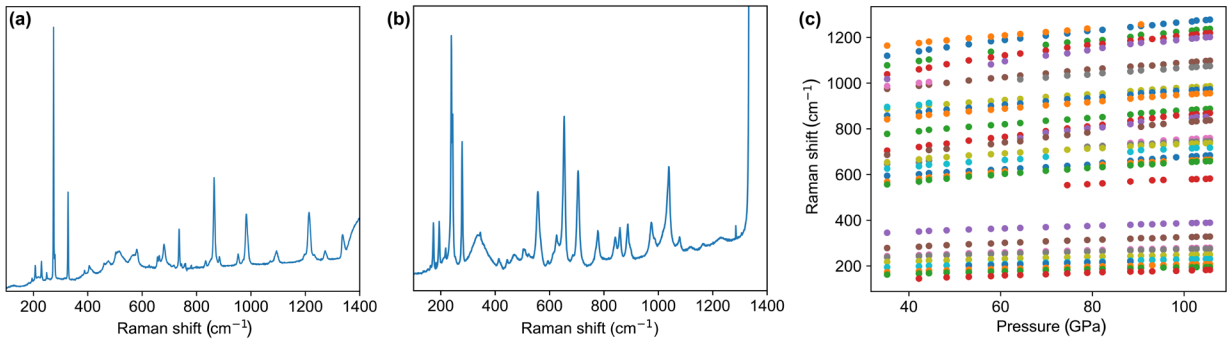

Figure S4. (a) Raman spectra of the Ta-N_2sample, laser-heated at ~105 GPa. (b) Raman spectrum of the Ta-N2 sample, laser-heated at ~105 GPa and decompressed to 35 GPa (c) Pressure dependence of Raman peaks on decompression.

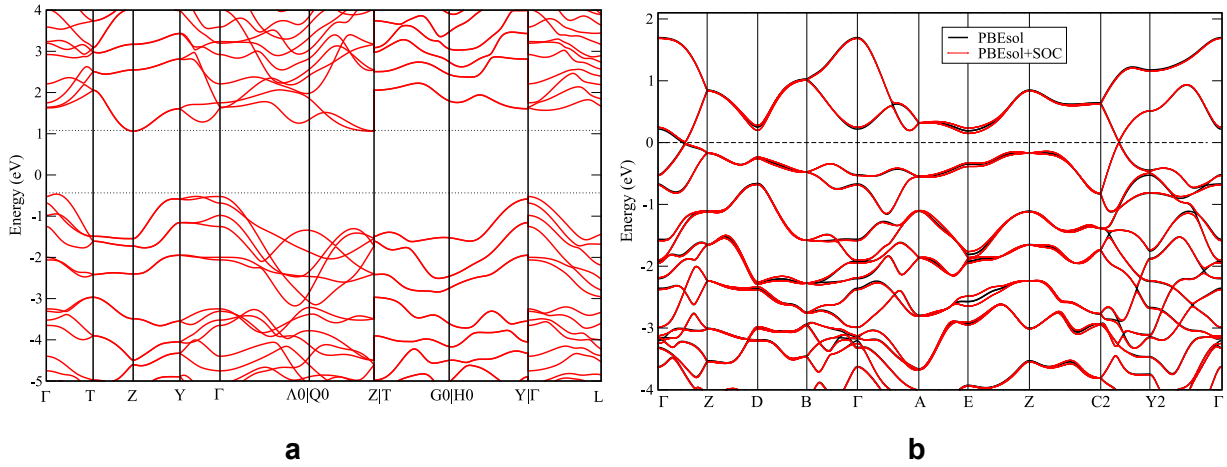

Figure S5. (left) The electronic band structure of TaN_5 at P ~ 105 GPa (V= 591.56 Å^3) calculated by PBEsol and (right) and the electronic band structure of TaN_4 at P ~ 102 GPa (V= 130.82 Å^3) calculated by PBEsol (black lines) and PBEsol including spin-orbit coupling (SOC).

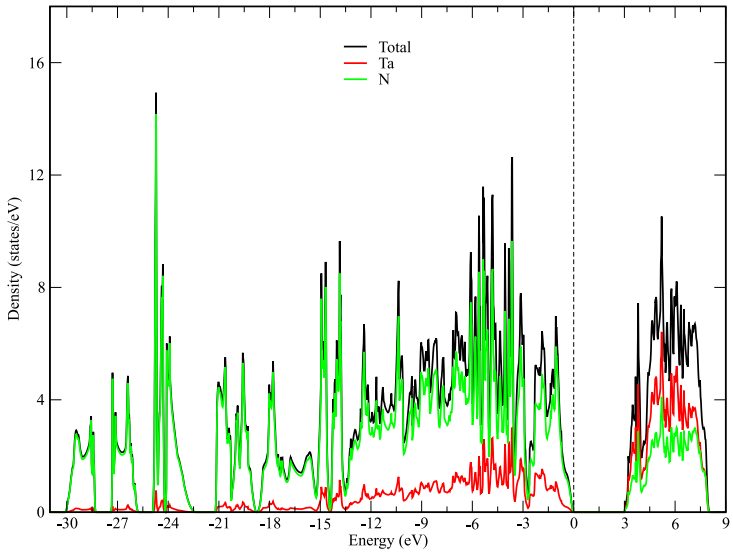

Figure S6. The calculated density of states of TaN_5 at volume V = 591.56 Å^3 calculated using HSE06.

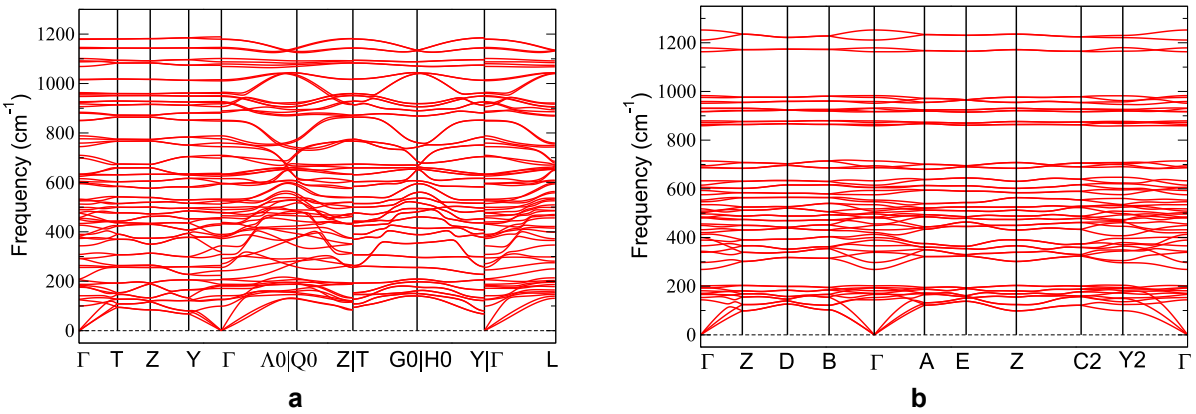

Figure S7. (a) The calculated phonon dispersions of TaN_5 at P=0 GPa, V=740 Å^3. (b) The calculated phonon dispersions of TaN_4 at P=0 GPa, V=166 Å^3 (right)

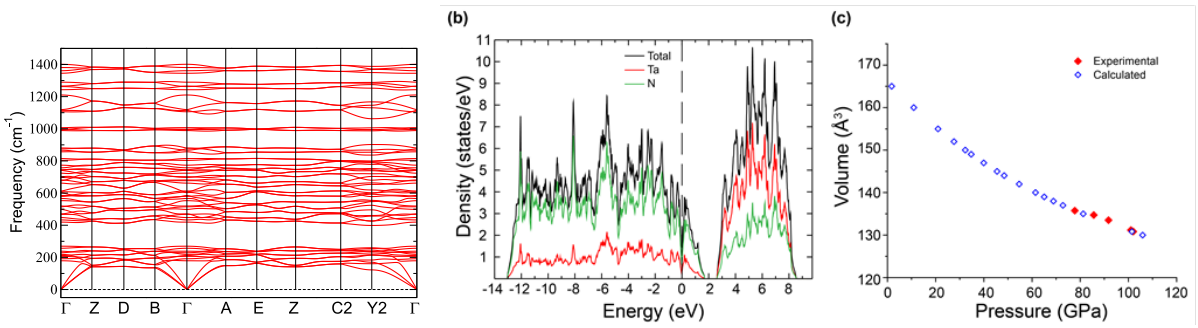

Figure S8. (a) The calculated phonon dispersions of TaN_4 at V=130.8 Å^3 and (b) The calculated electronic DoS the same pressure. (c) Experimental and calculated pressure-volume dependence of TaN_4 **(**can be described by the 3-rd order Birch-Murnaghan equation of state with V_0 = 166.9 Å^3, K_0 = 223.7 GPa, K' = 5.1**).**

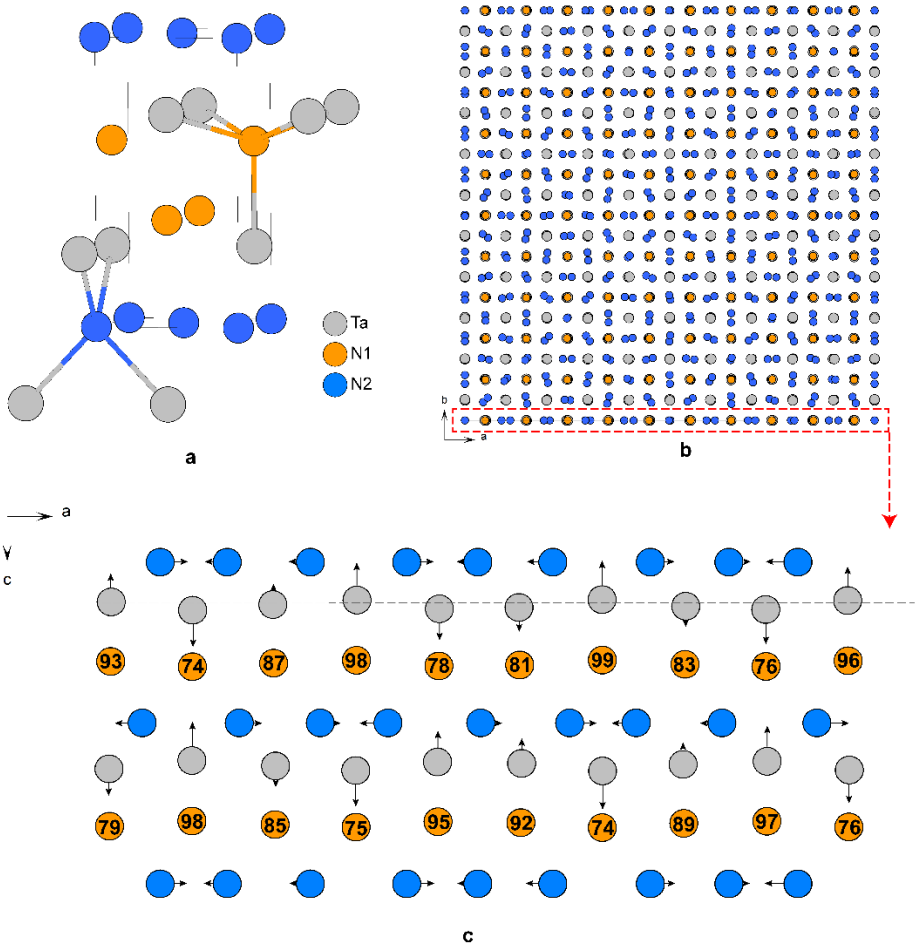

Figure S9. Crystal structure of TaN_{2-x} at 60 GPa. (a) Average structure (b) 10 × 10 × 2 approximant superstructure (c) Fragment of the approximant superstructure showing the atomic displacements and occupancies of N1 atoms in %. Arrows showing the atomic displacements are proportionally scaled for visibility. The average z-coordinate of Ta atoms is shown by a dashed gray line. Less occupied N1 sites lead to the displacements of neighboring Ta atoms towards this site, while fully occupied site "repel" the Ta atoms away. The N2 atoms follow the modulation of Ta atoms to prevent short N-N distances (Fig. 4c).

Table S1. Summary of laser-heating experiments

Sample	Pressure, GPa	Temperature, K	Products
#1	105	2020(200)	TaN_4, TaN_5
#1	62	2600(200)	$TaN_{1.86}$
#2	105	3300(200)	TaN_4, TaN_5
#3 *	32, 35, 40, 46, 51, 59	1400 – 3700	η-Ta_2N_3
#3	62	3200 (200)	TaN_{2-x}

* In the experiments with sample 3, upon pressure increase, both already reacted areas of the sample containing η-Ta_2N_3 and areas containing non-heated Ta were heated.

Table S2. Crystal structure and refinement details of TaN_4 and TaN_5

Chemical formula	TaN_4	TaN_5
Crystal system, space group	Monoclinic, $P2_1/n$	Orthorhombic, $Fdd2$
Temperature (K)	293	293
Pressure (GPa)	102	102
a, b, c (Å)	4.4564 (6), 5.4753 (4), 5.471 (4)	13.801(8), 11.8793(11), 3.6083(5)
β (°)	101.48 (3)	
V (Å^3)	130.82 (10)	591.6(4)
Z	4	16
Radiation type	Synchrotron, λ = 0.2901 Å	Synchrotron, λ = 0.2901 Å
μ (mm^{-1})	7.90	7.00
Data collection		
Diffractometer	LH@P02.2	LH@P02.2
No. of measured, independent and observed [$I > 2\sigma(I)$] reflections	774, 351, 340	560, 297, 288
R_{int}	0.028	0.03
$(\sin\theta/\lambda)_{max}$ (Å^{-1})	1.057	1.073
Refinement		
$R[F^2 > 2\sigma(F^2)]$, $wR(F^2)$, S	0.026, 0.065, 1.13	0.021, 0.051, 1.07
No. of reflections	351	297
No. of parameters	27	31
$\Delta\rho_{max}$, $\Delta\rho_{min}$ (e Å^{-3})	1.68, −2.05	1.92 / -1.73
Crystal structure	Ta1 (0.22684(6), 0.67436(3), 0.38011(10)) N1 (0.5510(12), 0.4464(8), 0.274(2)) N2 (0.7655(11), 0.5241(9), 0.156(2)) N3 (0.1239(13), 0.3149(7), 0.426(2)) N4 (-0.3404(13), 0.8401(7), 0.487(3))	Ta1 (0.17188(7), -0.67297(3), 0.4699(10)) N1 (0.045(2), -0.7711(7), 0.522(2)) N2 (0.302(2), -0.6778(8), 0.792(3)) N3 (0.297(2), -0.6777(8), 1.181(3)) N4 (0.045(2), -0.7625(9), 0.907(2)) N5 (0.3582(16), -0.5831(6), 0.718(4))

Table S3. Lattice parameters and unit cell volume of TaN_5 at different pressures

Pressure, GPa	***a*, Å**	***b*, Å**	***c*, Å**	***V*, Å^3**
102	13.801(8)	11.8793(11)	3.6083(5)	591.6(4)
101	13.848(5)	11.908(3)	3.605(2)	594.5(5)
91.75	13.979(7)	11.908(3)	3.6238(11)	603.2(4)
85.61	14.004(5)	12.021(6)	3.625(2)	610.3(6)
77.76	13.951(2)	12.097(8)	3.6413(9)	614.6(5)
60.97	14.132(4)	12.189(3)	3.675(2)	633.1(4)

Table S4. Lattice parameters and unit cell volume of TaN_4 at different pressures

Pressure, GPa	*a*, Å	*b*, Å	*c*, Å	β, º	*V*, Å^3
102	4.4564(6)	5.4753(4)	5.471(4)	101.48(3)	130.82(10)
101	4.4859(6)	5.4935(4)	5.428(4)	101.293(3)	131.17(12)
91.75	4.4915(15)	5.543(2)	5.461(2)	100.92(4)	133.52(9)
85.61	4.5129(15)	5.551(2)	5.476(2)	100.85(5)	134.72(9)
77.76	4.5007(18)	5.541(2)	5.546(4)	101.01(6)	135.76(14)

Table S5 Crystal structure and refinement details of $TaN_{1.863}$

Chemical formula	$TaN_{1.863}$
M_r	207
Crystal system, space group	Tetragonal, P4/*nmm*(αα½)0000(-αα½)0000 †
Temperature (K)	293
Pressure (GPa)	62
Wave vectors	$\mathbf{q}_1 = 0.305\mathbf{a}^* + 0.305\mathbf{b}^* + 0.5\mathbf{c}^*$; $\mathbf{q}_2 = -0.305\mathbf{a}^* + 0.305\mathbf{b}^* + 0.5\mathbf{c}^*$
a, *c* (Å)	2.8844(10), 5.723(2)
V (Å^3)	47.61(3)
Z	2
Radiation type	Synchrotron, λ = 0.2952 Å
μ (mm^{-1})	11.40
Data collection	
Diffractometer	13IDD @ APS
No. of measured, independent and observed [$I > 3\sigma(I)$] reflections	755, 259, 244
No. of observed independent main / satellite reflections	63/181
R_{int}	0.121
$(\sin\theta/\lambda)_{max}$ (Å^{-1})	0.874
Refinement	
$R[F^2 > 2\sigma(F^2)]$, $wR(F^2)$, S	0.073, 0.118, 9.78
No. of reflections	259
No. of parameters	15

† Symmetry operations: (1) x_1, x_2, x_3, x_4, x_5; (2) $-x_1, -x_2, x_3, x_3-x_4, x_3-x_5$; (3) $-x_2+1/2, x_1+1/2, x_3, x_3-x_5, x_4$; (4) $x_2+1/2, -x_1+1/2, x_3, x_5, x_3-x_4$; (5) $-x_1+1/2, x_2+1/2, -x_3, -x_3+x_5, -x_3+x_4$; (6) $x_1+1/2, -x_2+1/2, -x_3, -x_5, -x_4$; (7) $x_2, x_1, -x_3, -x_3+x_4, -x_5$; (8) $-x_2, -x_1, -x_3, -x_4, -x_3+x_5$; (9) $-x_1+1/2, -x_2+1/2, -x_3, -x_4, -x_5$; (10) $x_1+1/2, x_2+1/2, -x_3, -x_3+x_4, -x_3+x_5$; (11) $x_2, -x_1, -x_3, -x_3+x_5, -x_4$; (12) $-x_2, x_1, -x_3, -x_5, -x_3+x_4$; (13) $x_1, -x_2, x_3, x_3-x_5, x_3-x_4$; (14) $-x_1, x_2, x_3, x_5, x_4$; (15) $-x_2+1/2, -x_1+1/2, x_3, x_3-x_4, x_5$; (16) $x_2+1/2, x_1+1/2, x_3, x_4, x_3-x_5$.

Table S6. Structural parameters for the incommensurate TaN_{2-x} at ~62 GPa in a superspace group P4/*nmm*(αα½)0000(-αα½)0000 (No. 129.2.69.14). Modulation amplitudes are given using the fractional coordinate system.

Atom	Ta	N1	N2
x	0.5	0.5	0
y	0	0	0
z	0.266184	0.629859	0
U_{11} (Å^2)	0.005631	-	-
U_{22} (Å^2)	0.005631	-	-
U_{33} (Å^2)	0.006404	-	-
U_{12} (Å^2)	0	-	-
U_{13} (Å^2)	0	-	-
U_{23} (Å^2)	0	-	-
U_{iso} (Å^2)		0.003717	0.03049
A_x^{10}	0.005558	-0.00166	0.058027
A_y^{10}	0.005558	-0.00166	0.058027
A_z^{10}	-0.012458	-0.009669	0
B_x^{10}	-0.006154	-0.00384	0
B_y^{10}	-0.006154	-0.00384	0
B_z^{10}	-0.011252	0.004179	0
A_x^{01}	-0.005558	0.00166	-0.058027
A_y^{01}	0.005558	-0.00166	0.058027
A_z^{01}	-0.012458	-0.009669	0
B_x^{01}	0.006154	0.00384	0
B_y^{01}	-0.006154	-0.00384	0
B_z^{01}	-0.011252	0.004179	0
P^0	-	0.863124	-
P_s^{10}	-	0.056613	-
P_c^{10}	-	-0.024466	-
P_s^{01}	-	0.056613	-
P_c^{01}	-	-0.024466	-

Table S7. Lattice parameters of TaN_{2-x} at various pressures.

Pressure, GPa	*a*, Å	*c*, Å	**q**-vectors	V, Å^3
61	2.884(1)	5.723(2)	(0.305(1) 0.305(1) 0.5) (-0.305(1) 0.305(1) 0.5)	47.61(3)
0	3.0245(4)	5.9618(9)	(0.305(1) 0305(1) 0.5) (-0.305(1) 0.305(1) 0.5)	54.54(1)

References:

(1) Dewaele, A.; Loubeyre, P.; Mezouar, M. Equations of State of Six Metals above 94 GPa. *Phys. Rev. B* **2004**, *70* (9), 094112. https://doi.org/10.1103/PhysRevB.70.094112.

(2) Akahama, Y.; Kawamura, H. Pressure Calibration of Diamond Anvil Raman Gauge to 310 GPa. *J. Appl. Phys.* **2006**, *100* (4), 043516. https://doi.org/10.1063/1.2335683.

(3) Prescher, C.; Prakapenka, V. B. DIOPTAS: A Program for Reduction of Two-Dimensional X-Ray Diffraction Data and Data Exploration. *High Press. Res.* **2015**, *35* (3), 223–230. https://doi.org/10.1080/08957959.2015.1059835.

(4) Sheldrick, G. M. SHELXT – Integrated Space-Group and Crystal-Structure Determination. *Acta Crystallogr. Sect. A Found. Adv.* **2015**, *71* (1), 3–8. https://doi.org/10.1107/S2053273314026370.

(5) Petříček, V.; Dušek, M.; Plášil, J. Crystallographic Computing System Jana2006: Solution and Refinement of Twinned Structures. *Zeitschrift für Krist. - Cryst. Mater.* **2016**, *231* (10), 583–599. https://doi.org/10.1515/zkri-2016-1956.

(6) Dolomanov, O. V.; Bourhis, L. J.; Gildea, R. J.; Howard, J. A. K.; Puschmann, H. OLEX2: A Complete Structure Solution, Refinement and Analysis Program. *J. Appl. Crystallogr.* **2009**, *42* (2), 339–341. https://doi.org/10.1107/S0021889808042726.

(7) van Smaalen, S. *Incommensurate Crystallography*; Oxford University Press, 2007.

(8) Kresse, G.; Furthmüller, J. Efficiency of Ab-Initio Total Energy Calculations for Metals and Semiconductors Using a Plane-Wave Basis Set. *Comput. Mater. Sci.* **1996**, *6* (1), 15–50. https://doi.org/10.1016/0927-0256(96)00008-0.

(9) Kresse, G.; Furthmüller, J. Efficient Iterative Schemes for Ab Initio Total-Energy Calculations Using a Plane-Wave Basis Set. *Phys. Rev. B* **1996**, *54* (16), 11169–11186. https://doi.org/10.1103/PhysRevB.54.11169.

(10) Kresse, G.; Joubert, D. From Ultrasoft Pseudopotentials to the Projector Augmented-Wave Method. *Phys. Rev. B* **1999**, *59* (3), 1758–1775. https://doi.org/10.1103/PhysRevB.59.1758.

(11) Perdew, J. P.; Ruzsinszky, A.; Csonka, G. I.; Vydrov, O. A.; Scuseria, G. E.; Constantin, L. A.; Zhou, X.; Burke, K. Restoring the Density-Gradient Expansion for Exchange in Solids and Surfaces. *Phys. Rev. Lett.* **2008**, *100* (13), 136406.

https://doi.org/10.1103/PhysRevLett.100.136406.

(12) Heyd, J.; Scuseria, G. E.; Ernzerhof, M. Erratum: “Hybrid Functionals Based on a Screened Coulomb Potential” [J. Chem. Phys. 118, 8207 (2003)]. *J. Chem. Phys.* **2006**, *124* (21), 219906. https://doi.org/10.1063/1.2204597.

(13) Heyd, J.; Scuseria, G. E.; Ernzerhof, M. Hybrid Functionals Based on a Screened Coulomb Potential. *J. Chem. Phys.* **2003**, *118* (18), 8207–8215. https://doi.org/10.1063/1.1564060.

(14) Togo, A.; Tanaka, I. First Principles Phonon Calculations in Materials Science. *Scr. Mater.* **2015**, *108*, 1–5. https://doi.org/10.1016/j.scriptamat.2015.07.021.

(15) Pick, R. M.; Cohen, M. H.; Martin, R. M. Microscopic Theory of Force Constants in the Adiabatic Approximation. *Phys. Rev. B* **1970**, *1* (2), 910–920. https://doi.org/10.1103/PhysRevB.1.910.

(16) Giannozzi, P.; de Gironcoli, S.; Pavone, P.; Baroni, S. Ab Initio Calculation of Phonon Dispersions in Semiconductors. *Phys. Rev. B* **1991**, *43* (9), 7231–7242. https://doi.org/10.1103/PhysRevB.43.7231.

(17) Gonze, X.; Lee, C. Dynamical Matrices, Born Effective Charges, Dielectric Permittivity Tensors, and Interatomic Force Constants from Density-Functional Perturbation Theory. *Phys. Rev. B* **1997**, *55* (16), 10355–10368. https://doi.org/10.1103/PhysRevB.55.10355.